

Two distinct bifurcation routes for delayed optoelectronic oscillatorsLionel Weicker,^{1,2,*} Gaetan Friart,³ and Thomas Erneux³¹*Chair in Photonics, LMOPS, CentraleSupélec, Université Paris-Saclay, F-57070 Metz, France*²*Chair in Photonics, LMOPS, CentraleSupélec, Université de Lorraine, F-57070 Metz, France*³*Optique Nonlinéaire Théorique, Université Libre de Bruxelles, Campus Plaine, CP 231, 1050 Bruxelles, Belgium*

(Received 21 June 2017; published 7 September 2017)

We investigate the coexistence of low- and high-frequency oscillations in a delayed optoelectronic oscillator. We identify two nearby Hopf bifurcation points exhibiting low and high frequencies and demonstrate analytically how they lead to stable solutions. We then show numerically that these two branches of solutions undergo higher order instabilities as the feedback rate is increased but remain separated in the bifurcation diagram. The two bifurcation routes can be followed independently by either progressively increasing or decreasing the bifurcation parameter.

DOI: [10.1103/PhysRevE.96.032206](https://doi.org/10.1103/PhysRevE.96.032206)**I. INTRODUCTION**

Exploring, understanding, and controlling the effects of delayed feedbacks have become key issues in many areas of science and engineering [1–11]. In the life sciences, time delays can arise in the nervous system because of axonal conduction as in cell biology because of cell maturation times or in molecular biology because of the time required for transcription and translation. These delays may contribute to the generation of robust, clocklike oscillations [12] or, on the contrary, affect normal physiological functions [13,14]. In the manufacturing industry, delays in the metal cutting process are responsible for chatter instabilities characterized by violent vibrations, loud noise, and poor quality of surface finish [15]. In nonlinear optics, delayed optical feedbacks resulting from unwanted reflections are perturbing the normal output of semiconductor lasers (SLs) [16,17].

Modeling optical devices by delay differential equations (DDEs) started in 1979 when Ikeda predicted the existence of chaos in an optically bistable device [18,19]. It was then observed in a hybrid electro-optical system with computer-generated delay [20] and later in an all-optical system [21]. From then on, a large variety of long time oscillatory regimes were observed numerically and experimentally. Since most of the proposed models were exhibiting a delay much larger than any other time scale of the device, mathematicians became interested by the limit of large delays [22–26]. Particular attention was devoted to the first Hopf bifurcation which destabilizes the basic steady state. But other Hopf bifurcations are emerging from the unstable state as we continuously change our control parameter. A fundamental question is whether they may lead to stable oscillations past critical amplitudes. Nizette [27] showed that this is not likely to appear for the scalar first order DDEs treated by Ikeda and coworkers. More precisely, he examined the double limit of small amplitude solutions and large delays and showed that all primary Hopf branches of solutions except the first one are unstable. This, however, does not apply for optical systems described in terms of higher-order DDEs where multiple

stable oscillations of distinct periods have been identified both numerically [28–30] and experimentally [31,32]. Of particular physical interest is the coexistence of stable oscillations with periods of different magnitudes. Bifurcation mechanisms for this type of coexistence of periodic solutions of DDEs are not well understood. For a laser subject to a delayed optical feedback, we recently identified two Hopf bifurcation points with distinct frequencies responsible for one specific bifurcation scenario [30]. Here, we concentrate on delayed optoelectronic oscillators (OEOs) showing a similar coexistence of Hopf bifurcation points but leading to a different bifurcation scenario [33,34].

An OEO is a closed system capable of delivering a microwave electromagnetic wave of high spectral purity and of low electronic noise. Compared to lasers, OEOs are relatively recent devices [35]. The experimental setup of an OEO is schematically shown in Fig. 1. The feedback loop is sourced by means of a semiconductor continuous-wave laser injecting light into a Mach-Zehnder modulator (MZM). The nonlinearly modulated optical intensity at the MZM output is then sent through an optical fiber which is mainly responsible for the time delay τ . Subsequently, the light enters the optoelectronic feedback path where intensity fluctuations are detected by a broadband amplified photodiode (PD). This PD converts the nonlinearly transformed signal back into the electrical domain. The electrical signal is amplified (A), filtered (band-pass filter), and then used to drive the MZM [RF voltage $V(t)$], thus closing the feedback loop. Practically, the band-pass filter limits the overall bandwidth of the optoelectronic system and is determined by low and high cut-off times denoted by τ_L and τ_H , respectively. The interaction between nonlinearity and delay is responsible for a rich variety of dynamical phenomena. Because of the relative simplicity of the mathematical model and the good quantitative agreement with experiments, an OEO is a particularly desirable set up if we wish to explore delay-induced instabilities in the laboratory [36]. These instabilities and their control have led to new applications for secure optical communication [37], radars requiring ultra-pure sources of light [38–40], and neuromorphic computing [41,42].

For the laser subject to optical feedback [30], the coexistence of fast relaxation and slow square-wave oscillations were interpreted in terms of a simple harmonic oscillator subject to

*lionel.weicker@centralesupelec.fr

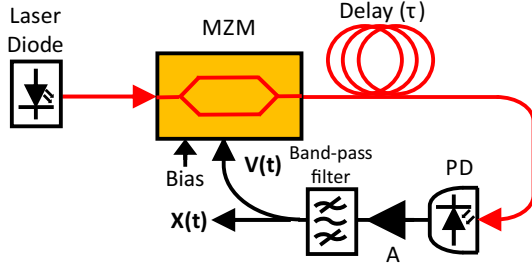


FIG. 1. Schematic of the experimental setup.

a delayed feedback described by

$$x'' + x = r[x(t - \tau) - x], \quad (1)$$

where r and τ denote the gain and the delay of the feedback, respectively. We found that the domain of stability of $x = 0$ is bounded by two Hopf bifurcations with either a frequency proportional to the inverse of the delay ($\omega_1 = \pi\tau^{-1}$) or the frequency of the harmonic oscillator ($\omega_2 = 1$). Here we consider another reference model more appropriate for the OEO oscillations. Specifically, we introduce the following second-order DDE

$$\varepsilon x'' + \varepsilon^2 x + x' - r x'(t - \tau) = 0, \quad (2)$$

where $\varepsilon \ll 1$ and r is the bifurcation parameter. By examining the stability properties of the zero solution, we find that the domain of stability is bounded by two Hopf bifurcation lines in the (r, τ) parameter space. In the limit $\varepsilon \rightarrow 0$, these Hopf bifurcations are given by

$$H_1 : r_0 \simeq 1 + \frac{\varepsilon^2 \tau}{2}, \quad \omega_0 \simeq \varepsilon \tau^{-1/2}, \quad (3)$$

$$H_2 : r_1 \simeq 1 + \frac{\varepsilon^2 2\pi^2}{\tau^2}, \quad \omega_1 \simeq 2\pi \tau^{-1}(1 - \varepsilon), \quad (4)$$

and are represented in Fig. 2.

The first instability (H_1) dominates for low values of τ and requires progressively larger values of $r - 1$ as τ increases. On the other hand, the second instability (H_2) takes over for τ sufficiently large and requires progressively lower values

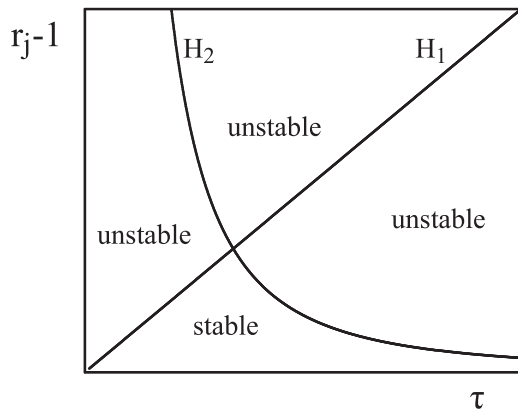


FIG. 2. The stability of the zero solution is bounded by the Hopf bifurcation lines H_1 and H_2 given by (3) and (4), respectively. Stable and unstable mean that the zero solution is either stable or unstable.

of $r - 1$. This behavior is typical of many delayed feedback problems where the Hopf bifurcation is induced by the delay: increasing the delay allows to reduce the critical feedback rate for a Hopf bifurcation.

The plan of the paper is as follows. In the next section, we formulate the equations for an OEO and determine the two first Hopf bifurcations. For the parameters values used in Ref. [34], the critical feedback rates of these Hopf bifurcation points exhibits nearby values and motivates a two parameter bifurcation analysis close to a double Hopf bifurcation point. The details are described in Sec. III. In Sec. IV, we substantiate our analytical results by investigating numerically the bifurcation diagram from low to large values of the control parameter. Finally, we discuss in Sec. V earlier observations of low- and high-frequency oscillations of an OEO [33].

II. FORMULATION

OEOs are described mathematically by two first-order delay differential equations of the form (see Ref. [43])

$$\tau_L \frac{dx}{dt} = -\left(1 + \frac{\tau_L}{\tau_H}\right)x - y - \beta \cos^2[x(t - \tau) + \phi], \quad (5)$$

$$\tau_H \frac{dy}{dt} = x, \quad (6)$$

where x is the normalized output signal representing the voltage applied to the modulator, β is a dimensionless parameter which describes the feedback strength of the loop, τ is the total delay of the feedback signal, and ϕ is the bias point of the modulator. τ_L and τ_H are time constants describing the low-pass and high-pass filters [the low-pass cut-off and high-pass cut-on frequencies are $1/(2\pi\tau_L)$ and $1/(2\pi\tau_H)$, respectively]. By introducing the dimensionless time $s = t/\tau$ and after differentiating Eq. (5) in order to eliminate y , using Eq. (6), we obtain the following dimensionless equation:

$$\frac{\gamma x''}{\delta} + x'(1 + \gamma) + \delta x = \beta \sin[2x(s - 1) + 2\phi]x'(s - 1), \quad (7)$$

where prime means differentiation with respect to s . The dimensionless parameters γ and δ are defined as $\gamma \equiv \tau_L/\tau_H$ and $\delta \equiv \tau/\tau_H$. Using the parameters listed in Ref. [34], namely,

$$\phi = \pi/4, \quad \tau = 22.5 \text{ ns}, \quad \tau_H = 0.16 \text{ } \mu\text{s}, \text{ and } \tau_L = 1.6 \text{ ns}, \quad (8)$$

we find

$$\gamma = 10^{-2} \quad \text{and} \quad \delta = 0.1411. \quad (9)$$

Equation (7) with $\phi = \pi/4$ simplifies as

$$\frac{\gamma x''}{\delta} + x'(1 + \gamma) + \delta x = \beta \cos[2x(s - 1)]x'(s - 1). \quad (10)$$

This equation admits a single steady state $x = 0$. From the linearized equation, we determine the characteristic equation for the growth rate σ given by

$$\gamma \delta^{-1} \sigma^2 + \sigma(1 + \gamma) + \delta - \beta \sigma \exp(-\sigma) = 0. \quad (11)$$

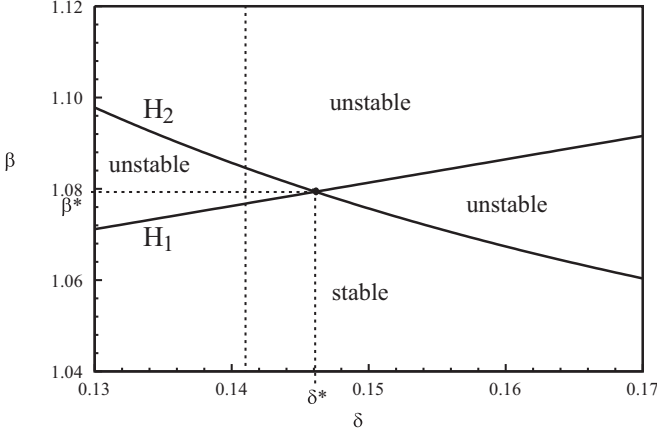


FIG. 3. The two first Hopf bifurcation lines H_1 and H_2 in the β versus δ stability diagram. They have been obtained by determining $\delta = \delta(\omega)$ from Eq. (14) and then β using Eq. (13). The two Hopf bifurcation lines intersect at $(\delta, \beta) = (\delta^*, \beta^*) = (0.146, 1.079)$. The vertical broken line at $\delta = 0.1411$ marks the value used in Ref. [34]. The values of the fixed parameters are $\phi = \pi/4$ and $\gamma = 10^{-2}$. The first and second Hopf bifurcations are characterized by a frequency $\omega_1 \ll 1$ and by a frequency $\omega_2 \simeq 2\pi$, respectively. Stable and unstable mean that the steady state is stable and unstable, respectively.

In order to determine the conditions for a Hopf bifurcation point, we insert $\sigma = i\omega$ into Eq. (11) and separate the real and imaginary parts. We find the following two conditions for the bifurcation point in terms of β and the frequency ω of the oscillations at the bifurcation point

$$-\gamma\delta^{-1}\omega^2 + \delta = \beta\omega \sin(\omega), \quad (12)$$

$$(1 + \gamma) = \beta \cos(\omega). \quad (13)$$

By eliminating β , we obtain an equation for $\omega = \omega(\delta, \gamma)$ of the form

$$-\delta^2 + \delta\omega(1 + \gamma) \tan(\omega) + \gamma\omega^2 = 0. \quad (14)$$

γ is kept fixed. We treat $\omega > 0$ as a parameter and solve the quadratic equation (14) for δ and Eq. (13) for β . Figure 3 represents the two first Hopf bifurcation lines in the (δ, β) stability diagram. We note that the two lines intersect at $\delta = \delta^*$. The critical point $(\delta, \beta) = (\delta^*, \beta^*)$ is a codimension two Hopf bifurcation point characterized by two distinct pairs of imaginary eigenvalues ($\pm i\omega_1$ and $\pm i\omega_2$). We determine the coordinates of this point by realizing from Eq. (13) with $\beta = \beta^*$ that

$$\cos(\omega_1) = \cos(\omega_2). \quad (15)$$

The solution of Eq. (15) that is matching our numerical estimate of $\omega_1 \simeq 0.36$ and $\omega_2 \simeq 5.92$ is

$$\omega_2 = 2\pi - \omega_1. \quad (16)$$

Equation (14) with $\delta = \delta^*$ is then evaluated for $\omega = \omega_1$ and for $\omega = 2\pi - \omega_1$ providing two conditions for ω_1

$$\gamma\omega_1^2 + (1 + \gamma)\omega_1\delta^* \tan(\omega_1) = \delta^{*2}, \quad (17)$$

$$\gamma(2\pi - \omega_1)^2 - (1 + \gamma)(2\pi - \omega_1)\delta^* \tan(\omega_1) = \delta^{*2}. \quad (18)$$

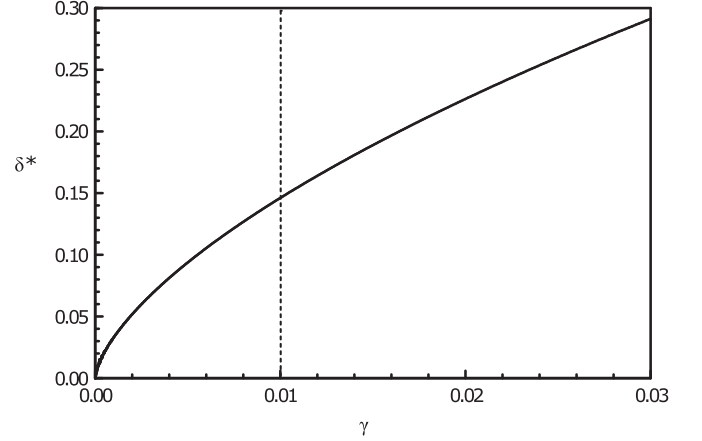


FIG. 4. Critical δ^* for a double Hopf bifurcation point as a function of γ . It has been obtained by first determining $\omega_1 = \omega_1(\gamma)$ from Eq. (20) and then by evaluating δ^* from Eq. (19). The vertical broken line denotes the value of $\gamma = 10^{-2}$ used in Ref. [34].

By subtracting these two equations, we eliminate δ^{*2} and find an expression for $\delta^* = \delta^*(\omega_1)$ which reads as

$$\delta^* = \frac{\gamma(2\pi - 2\omega_1)}{(1 + \gamma) \tan(\omega_1)}. \quad (19)$$

Substituting (19) into Eq. (17), and simplifying, we obtain the following quadratic equation for $\gamma = \gamma(\omega_1)$

$$\gamma^2 + 2\gamma \left\{ 1 - 2 \left[\frac{\pi - \omega_1}{\tan(\omega_1)} \right]^2 \frac{1}{\omega_1 2\pi - \omega_1^2} \right\} + 1 = 0. \quad (20)$$

An analysis of the real roots of Eq. (20) indicates that $\omega_1(\gamma)$ emerges from zero, reaches a maximum at $\gamma = 1$ ($\omega_{1m} = 0.7594$) and then decreases as γ is further increased. Figure 4 represents the critical value δ^* as function of γ . Since $\gamma = 10^{-2}$ in Ref. [34], the limit $\gamma \rightarrow 0$ is instructive. From Eq. (20), the leading expression for ω_1 is

$$\omega_1 = (2\pi\gamma)^{1/3}. \quad (21)$$

If $\delta < \delta^*$, then the first Hopf bifurcation is H_1 and leads to low-frequency oscillations because ω_1 is small. If $\delta > \delta^*$, then the first Hopf bifurcation is H_2 and leads to nearly 1-periodic oscillations because $\omega_2 = 2\pi - \omega_1 \simeq 2\pi$. Our bifurcation problem is therefore characterized by the interaction of two time-periodic modes operating on different time scales. This situation is the same as the one shown in Fig. 2 for our toy model (2).

III. HOPF-HOPF BIFURCATION

We propose to determine the solutions in the vicinity of $(\beta, \delta) = (\beta^*, \delta^*)$ by a two-parameter weakly nonlinear analysis. To this end, we first introduce a small parameter ε defined as

$$\varepsilon = \sqrt{\frac{\delta - \delta^*}{c}}, \quad (c = \pm 1) \quad (22)$$

and expand β as

$$\beta = \beta^* + \varepsilon^2 \beta_2 + \dots \quad (23)$$

We next seek a solution of the form

$$x = \varepsilon x_1(s, \theta) + \varepsilon^2 x_2(s, \theta) + \varepsilon^3 x_3(s, \theta) + \dots, \quad (24)$$

where $\theta \equiv \varepsilon^2 s$ is defined as a slow time variable. The method of multiple time scales treats the two times s and θ as independent variables [44,45]. Consequently, we need the chain rules

$$\begin{aligned} x' &= x_s + \varepsilon^2 x_{s\theta} + O(\varepsilon^4), \\ x'' &= x_{ss} + 2\varepsilon^2 x_{s\theta} + O(\varepsilon^4), \end{aligned} \quad (25)$$

where the subscripts s and θ means partial derivatives. We also need to expand the delayed variable which now depends on two times

$$x(s-1) = x(s-1, \theta) - \varepsilon^2 x_{\theta}(s-1, \theta) + O(\varepsilon^4). \quad (26)$$

Inserting (22)–(26) into Eq. (10), we equate to zero the coefficients of each power of ε . We obtain a sequence of linear problems for the functions $x_j(s, \theta)$. The three first problems are given by

$$Lx_1 \equiv \gamma \delta^{*-1} x_{1ss} + x_{1s}(1 + \gamma) + \delta^* x_1 - \beta^* x_{1s}(s-1) = 0, \quad (27)$$

$$Lx_2 = 0, \quad (28)$$

$$\begin{aligned} Lx_3 = & \left[\beta_2 x_{1s}(s-1) + \gamma \frac{c}{\delta^{*2}} x_{1ss} - cx_1 \right. \\ & - 2\beta^* x_1^2(s-1) x_{1s}(s-1) - 2\gamma \delta^{*-1} x_{1s\theta} - x_{1\theta}(1 + \gamma) \\ & \left. + \beta^* [x_{1\theta}(s-1) - x_{1s\theta}(s-1)] \right], \end{aligned} \quad (29)$$

Equations (27) and (28) admit the following solutions:

$$x_1 = A_1 \exp(i\omega_1 s) + A_2 \exp(i\omega_2 s) + \text{c.c.}, \quad (30)$$

$$x_2 = B_1 \exp(i\omega_1 s) + B_2 \exp(i\omega_2 s) + \text{c.c.}, \quad (31)$$

where ω_1 and ω_2 are the Hopf frequencies at $\delta = \delta^*$. A_1 , A_2 , B_1 , and B_2 are four unknown amplitudes which depend of θ . To find them, we need to explore the higher-order problems for x_j and apply solvability conditions. Because the equations for x_j are scalar, these conditions require that the coefficients of $\exp(\pm i\omega_1 s)$ and $\exp(\pm i\omega_2 s)$ in the right-hand side must be zero in order to avoid secular terms in the solution. From Eq. (29) with $A_j = R_j \exp(i\phi)$, these conditions lead to two ordinary differential equations for R_1 and R_2 given by

$$R_1' = (-\beta_2 a_1 + cb_1) R_1 + 2\beta^* a_1 (R_1^2 + 2R_2^2) R_1, \quad (32)$$

$$R_2' = (-\beta_2 a_2 + cb_2) R_2 + 2\beta^* a_2 (R_2^2 + 2R_1^2) R_2, \quad (33)$$

where prime now means differentiation with respect to the slow time θ and

$$a_j = \text{Re} \left[\frac{i\omega_j \exp(-i\omega_j)}{c_j} \right], \quad (34)$$

$$b_j = \text{Re} \left(\frac{\gamma \delta^{*-2} \omega_j^2 + 1}{c_j} \right), \quad (35)$$

where

$$c_j = -2\gamma \delta^{*-1} i\omega_j - (1 + \gamma) + \beta^* e^{-i\omega_j} - \beta^* i\omega_j e^{-i\omega_j}. \quad (36)$$

The coefficients a_j and b_j are evaluated in the appendix. We demonstrate that

$$b_j = \beta_{2j} a_j / c \quad \text{and} \quad a_j < 0, \quad (37)$$

where $\beta_{2j} = \beta_{2j}(c)$ comes from the expansion of the Hopf bifurcation points near $\beta = \beta^*$ (see Appendix). Equations (32) and (33) may then be rewritten as

$$R_1' = -a_1(\beta_2 - \beta_{21}) R_1 + 2\beta^* a_1 (R_1^2 + 2R_2^2) R_1, \quad (38)$$

$$R_2' = -a_2(\beta_2 - \beta_{22}) R_2 + 2\beta^* a_2 (R_2^2 + 2R_1^2) R_2. \quad (39)$$

Equations (38) and (39) admit four steady states: the zero solution, two pure mode solutions, and one mixed mode solution. The pure mode solutions are

$$(1): \quad R_1^2 = \frac{\beta_2 - \beta_{21}}{2\beta^*} \geq 0 \quad \text{and} \quad R_2 = 0, \quad (40)$$

$$(2): \quad R_1 = 0 \quad \text{and} \quad R_2^2 = \frac{\beta_2 - \beta_{22}}{2\beta^*} \geq 0, \quad (41)$$

and the mixed mode solution is

$$R_1^2 = \frac{\beta_2 + \beta_{21} - 2\beta_{22}}{6\beta^*} \geq 0, \quad (42)$$

$$R_2^2 = \frac{\beta_2 - 2\beta_{21} + \beta_{22}}{6\beta^*} \geq 0. \quad (43)$$

If $c = -1$, which is the case in Ref. [34] ($\delta < \delta^*$), then $\beta_{21} < 0$ and $\beta_{22} > 0$ according to (A4). Consequently, (43) is always positive if $\beta_2 > 0$ and from (42) we have the inequality

$$\beta_2 > \beta_{23} \equiv -\beta_{21} + 2\beta_{22} > 0. \quad (44)$$

The critical point $\beta_2 = \beta_{23}$ is a secondary bifurcation point from the pure mode solution (41) to the mixed mode solution (42) and (43). The linear stability of all solutions can be determined from Eqs. (38) and (39). In Fig. 5(a), we represent the bifurcation diagram of the pure and mixed mode solutions when $c = -1$. The pure mode (40), characterized by low frequency oscillations, emerges from β_{21} and is noted 1 whereas the pure mode (41) leading to a delay-periodic regime, emerges from β_{22} and is noted 2. The mixed mode solutions [(42) and (43)] are denoted by 1 + 2 and appears for $\beta_2 \geq \beta_{23}$.

A similar bifurcation diagram appears if $c = 1$ and is shown in Fig. 5(b). The secondary bifurcation point is now given by

$$\beta_{23} \equiv -\beta_{22} + 2\beta_{21}. \quad (45)$$

The stability of the different solutions are represented by broken lines (unstable) and straight (stable) lines. We conclude that the coexistence between two stable pure time-periodic solutions is always possible provided $\beta_2 \geq \beta_{23}$.

IV. NUMERICAL SIMULATIONS

We anticipate that the emergence of these two stable branches of periodic solutions exhibiting different periods are leading to distinct routes of more complex oscillations. This

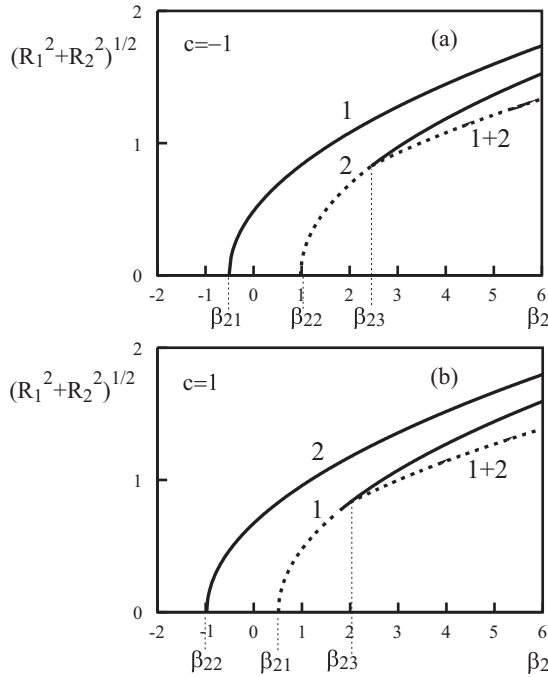


FIG. 5. Bifurcation diagram of the steady-state solutions of Eqs. (38) and (39). Panels (a) and (b) illustrate the case $c = -1$ and $c = 1$, respectively. Both cases allow the coexistence of stable pure mode solutions through a secondary bifurcation mechanism.

scenario is substantiated by systematic numerical simulations of Eqs. (5) and (6). Specifically, we numerically investigate the stable solutions using a fourth-order Runge-Kutta algorithm. The initial conditions for the first simulation are $x = 0.06$ and $y = 0.41$ ($-1 < s < 0$). The bifurcation parameter is then progressively increased by small steps using the previous solution as the initial conditions for the time interval ($-1 < s < 0$). The same procedure is applied when we progressively decrease the bifurcation parameter. By progressively changing the feedback strength β , we determine the bifurcation diagram

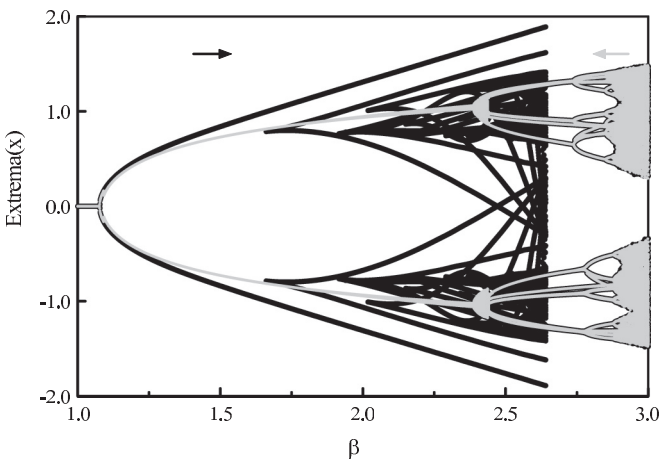


FIG. 6. Bifurcation diagrams of the extrema of x obtained numerically from Eqs. (5) and (6) by progressively increasing (black) or decreasing (gray) β . The fixed parameters are $\phi = \pi/4$, $\delta = 0.1411$, and $\gamma = 10^{-2}$.

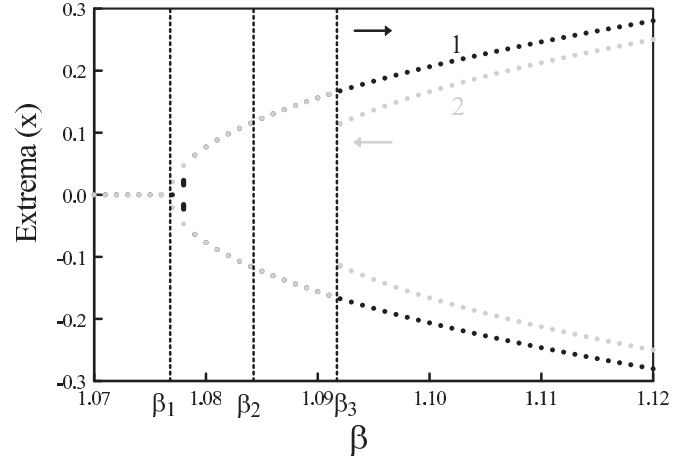


FIG. 7. Blow-up of the bifurcation diagrams near the two first Hopf bifurcations. Branch 1 (black dots) and Branch 2 (gray dots) correspond to the forward diagram of Fig. 6 (black line) and the backward diagram of Fig. 6 (gray line), respectively.

for the extrema of x as function of β with the fixed parameters used in Ref. [34]. See Fig. 6.

By progressively increasing β from 1 to 3 (in black), a supercritical Hopf bifurcation at $\beta \simeq 1.077$ marks the transition between a stable steady state and stable periodic oscillations. The single frequency oscillations are observed until $\beta = 1.66$. Increasing further β then leads to multiperiodic and chaotic regimes. The chaotic oscillations exhibit two distinct time scales and recall the chaotic breathers studied in Ref. [33]. Near $\beta \simeq 2.65$, the oscillations are getting close to the unstable zero solution and we observe an abrupt transition to another attractor.

When we progressively decrease β from 3 to 2.7 (in gray), the long time numerical solutions are first identical to those obtained when we increased β from $\beta = 2.7$ to 3. Below $\beta = 2.7$, we however follow a different route. If $\beta < 2.45$, then the system exhibits single frequency periodic oscillations until it shows a transition to a stable steady state near $\beta = 1.077$.

Figure 7 is a blow-up of the bifurcation diagram in the vicinity of the two first Hopf bifurcation points. The branches denoted by 1 (black) and by 2 (gray) correspond to the bifurcation diagrams obtained by increasing and then decreasing β , respectively. As predicted by our analysis [see Fig. 5(a)], two distinct branches of stable periodic solutions are emerging from the steady state $x = 0$. Branch 1 is leading to low frequency oscillations ($P = 15-20$) while Branch 2 exhibits oscillations of period close to the delay ($P = 1$). The bifurcation points β_1 , β_2 , and β_3 are defined as $\beta_j = \beta^* + \varepsilon^2 \beta_{2j}$ where the β_{2j} were documented in the previous section. They mark the first Hopf bifurcation (β_1), the second primary Hopf bifurcation (β_2), and the secondary bifurcation responsible for the change of stability of Branch 2 (β_3). We note a good quantitative agreement between the analytical and numerical values of β_1 and β_3 .

V. DISCUSSION

In summary, we found that the bifurcation diagram of a class of OEOs is organized in terms of two distinct branches

of solutions each starting from a Hopf bifurcation point with a different frequency. Both our analysis and simulations were based on parameters documented by Cohen *et al.* [34]. Their values are close to the coordinates of a degenerated Hopf bifurcation which is the starting point of our weakly nonlinear analysis. If we deviate from this particular point, we expect that the bifurcation diagram will remain qualitatively unchanged. Only the secondary bifurcation points will appear at higher amplitudes. The toy model Eq. (2) is the linearized equation of (7). It emphasizes the small values of the coefficients multiplying the first two terms and their relative scaling. The direction of bifurcation however depends on the nonlinear terms which, in the case of Eq. (7), always leads to supercritical bifurcations.

Earlier work by Chembo *et al.* [33] showed a similar bifurcation diagram. Specifically, the first Hopf bifurcation appears very close to $\beta = 1$ and leads to oscillations with a frequency close to 2π . As soon as $\beta = 1.003$, a stable attractor of frequency close to $\sqrt{\delta}$ is possible if the initial conditions were chosen close to the unstable steady state. From their parameter values, we compute $\gamma = 5 \times 10^{-6}$ and $\delta = 6 \times 10^{-3}$. We find that the two first Hopf bifurcation points coalesce at $(\delta^*, \beta^*) = (9.905 \times 10^{-4}, 1.0005)$ with the two frequencies $\omega_1 = 0.039$ and $\omega_2 = 6.252$. Since $\delta > \delta^*$, the case $c = 1$ applies [see Fig. 5(b)]. Our bifurcation analysis predicts that the low frequency oscillations appears at the second primary Hopf bifurcation whereas the delay-periodic solution emerges at the first primary Hopf bifurcation.

Note that the values of δ and γ are much lower than the values (9) used in Ref. [34]. As observed in Ref. [33] and explained later in Ref. [43], the low values of δ and γ are generating slow-fast oscillations if the amplitude of the oscillations is sufficiently large causing new bifurcations to hybrid slow-fast oscillations.

The coexistence of branches of solutions exhibiting distinct periods seems a natural phenomenon for oscillators subject to a delayed feedback when the delay is sufficiently large. Both in Ref. [30] and here, we explain this coexistence by identifying specific Hopf bifurcation points. In Ref. [30], the first Hopf bifurcation leads to a branch of fast laser relaxation oscillations and is followed by a branch of slower 2τ -periodic square waves. However, the problem was mathematically too complex for analysis and we could not explain why the second branch becomes stable past a critical amplitude. Here, we showed how the second primary branch gets stabilized through a secondary bifurcation mechanism by unfolding a degenerate Hopf bifurcation point.

ACKNOWLEDGMENTS

L.W. acknowledges the support of Conseil Régional Grand-Est, of Agence Nationale de la Recherche (ANR) through the TINO project (ANR12-JS03-005), of Fondation Supélec, Metz Métropole, Conseil Départemental Moselle, Airbus-GDI Simulation, and Préfecture de Région Grand-Est, FEDER through the Chair in Photonics and PIANO (FNADT) project. T.E. is grateful of the support of the F.N.R.S. This work also benefited from the support of the Belgian Science Policy Office under Grant No IAP-7/35 photonics@be.

APPENDIX

We first determine expressions for the primary Hopf bifurcation points close to $(\beta, \delta) = (\beta^*, \delta^*)$. By inserting

$$\beta = \beta^* + \varepsilon^2 \beta_{2j},$$

$$\delta = \delta^* + \varepsilon^2 c,$$

$$\omega = \omega_j + \varepsilon^2 \Omega_j$$

into the Hopf conditions (12) and (13), we obtain the following relations between β_{2j} , c , and Ω_j :

$$\left[\begin{array}{l} (\gamma \delta^{*-2} \omega_j^2 + 1)c - \beta_{2j} \omega_j \sin(\omega_j) \\ -\Omega_j \{\gamma \delta^{*-1} 2\omega_j + \beta^* [\sin(\omega_j) + \omega_j \cos(\omega_j)]\} \end{array} \right] = 0, \quad (\text{A1})$$

$$-\beta^* \sin(\omega_j) \Omega_j + \beta_{2j} \cos(\omega_j) = 0. \quad (\text{A2})$$

Using (A2), we eliminate Ω_j in Eq. (A1) and obtain an equation for $\beta_{2j} = \beta_{2j}(c)$ given by

$$(\gamma \delta^{*-2} \omega_j^2 + 1)c = \frac{\beta_{2j}}{\beta^* \sin(\omega_j)} \left[\begin{array}{l} \beta^* \omega_j + \gamma \delta^{*-1} 2\omega_j \cos(\omega_j) \\ + \beta^* \sin(\omega_j) \cos(\omega_j) \end{array} \right].$$

This equation will be useful when we evaluate b_j . The expression in the square brackets can be simplified. We use (12) evaluated at $(\beta, \delta) = (\beta^*, \delta^*)$ and eliminate $\sin(\omega_j)$ in the bracket. We obtain

$$\beta_{2j} = \frac{\beta^* \sin(\omega_j) (\gamma \delta^{*-2} \omega_j^2 + 1)c}{\beta^* \omega_j + (\gamma \delta^{*-1} \omega_j + \frac{\delta^*}{\omega_j}) \cos(\omega_j)}. \quad (\text{A3})$$

The denominator is always positive since from (13) $\cos(\omega_j) > 0$. Therefore the sign of β_{2j} is determined by the sign of $c \sin(\omega_j)$. Recall that $\omega_1 < \pi/2$ and $\omega_2 = 2\pi - \omega_1$. Consequently,

$$\text{sgn}(\beta_{21}) = \text{sgn}(c),$$

$$\text{sgn}(\beta_{22}) = \text{sgn}(-c). \quad (\text{A4})$$

We next consider c_j defined by Eq. (36) as

$$c_j = -2\gamma \delta^{*-1} i \omega_j - (1 + \gamma) + \beta^* e^{-i\omega_j} - \beta^* i \omega_j e^{-i\omega_j}. \quad (\text{A5})$$

From Eq. (11), we find an expression for $\beta^* e^{-i\omega_j}$ given by

$$\beta^* e^{-i\omega_j} = i\gamma \delta^{*-1} \omega_j + (1 + \gamma) - \frac{i\delta^*}{\omega_j},$$

which allow to simplify c_j , given by (A5), as

$$c_j = -i\omega_j \left[\gamma \delta^{*-1} + \frac{\delta^*}{\omega_j^2} + \beta^* e^{-i\omega_j} \right]. \quad (\text{A6})$$

Introducing (A6) into the expression for a_j , defined by Eq. (34), we find

$$a_j = \text{Re} \left[-\frac{\exp(-i\omega_j)}{\gamma \delta^{*-1} + \frac{\delta^*}{\omega_j^2} + \beta^* \exp(-i\omega_j)} \right] \\ = -\frac{(\gamma \delta^{*-1} + \frac{\delta^*}{\omega_j^2}) \cos(\omega_j) + \beta^*}{(\gamma \delta^{*-1} + \frac{\delta^*}{\omega_j^2})^2 + 2\beta^* (\gamma \delta^{*-1} + \frac{\delta^*}{\omega_j^2}) \cos(\omega_j) + \beta^{*2}},$$

which is clearly negative since $\cos(\omega_j) = (1 + \gamma)/\beta^* > 0$. Similarly, we introduce (A6) into the expression for b_j given by Eq. (35) and find

$$b_j = \operatorname{Re} \left\{ \frac{\gamma \delta^{*-2} \omega_j^2 + 1}{-i \omega_j \left[\gamma \delta^{*-1} + \frac{\delta^*}{\omega_j^2} + \beta^* \exp(-i \omega_j) \right]} \right\} = \frac{-\frac{1}{\omega_j} \beta^* \sin(\omega_j) (\gamma \delta^{*-2} \omega_j^2 + 1)}{(\gamma \delta^{*-1} + \frac{\delta^*}{\omega_j^2})^2 + 2\beta^* (\gamma \delta^{*-1} + \frac{\delta^*}{\omega_j^2}) \cos(\omega_j) + \beta^{*2}}.$$

Using (A3), we can rewrite this equation as

$$b_j = \frac{-[\beta^* + (\gamma \delta^{*-1} + \delta^*/\omega_j^2) \cos(\omega_j)] \beta_{2j}/c}{(\gamma \delta^{*-1} + \frac{\delta^*}{\omega_j^2})^2 + 2\beta^* (\gamma \delta^{*-1} + \frac{\delta^*}{\omega_j^2}) \cos(\omega_j) + \beta^{*2}} = a_j \beta_{2j}/c.$$

-
- [1] T. Erneux, *Applied Delay Differential Equations* (Springer Science & Business Media, Berlin, 2009), Vol. 3.
- [2] G. Stepan, *Philos. Trans. R. Soc. Lond. A* **367**, 1059 (2009).
- [3] B. Balachandran, T. Kalmár-Nagy, and D. E. Gilsinn, *Delay Differential Equations* (Springer, Berlin, 2009).
- [4] F. M. Atay, *Complex Time-Delay Systems: Theory and Applications* (Springer, Berlin, 2010).
- [5] H. Smith, *An Introduction to Delay Differential Equations with Applications to the Life Sciences* (Springer Science & Business Media, Berlin, 2010), Vol. 57.
- [6] W. Just, A. Pelster, M. Schanz, and E. Schöll, *Philos. Trans. R. Soc. Lond. A* **368**, 303 (2009).
- [7] M. Lakshmanan and D. V. Senthilkumar, *Dynamics of Nonlinear Time-Delay Systems* (Springer Science & Business Media, Berlin, 2011).
- [8] T. Insperger and G. Stépán, *Semi-Discretization for Time-Delay Systems: Stability and Engineering Applications* (Springer Science & Business Media, Berlin, 2011), Vol. 178.
- [9] J. Milton and T. Ohira, *Mathematics as a Laboratory Tool* (Springer, Berlin, 2014).
- [10] M. C. Mackey, M. Santillán, M. Tyran-Kamińska, and E. S. Zeron, *Simple Mathematical Models of Gene Regulatory Dynamics* (Springer, Berlin, 2016).
- [11] E. Witrant, E. Fridman, O. Senane, and L. Dugard, *Recent Results on Time-Delay Systems: Analysis and Control* (Springer, Berlin, 2016), Vol. 5.
- [12] Q. Yang and J. E. Ferrell Jr., *Nat. Cell Biol.* **15**, 519 (2013).
- [13] L. Glass, *Chaos* **25**, 097603 (2015).
- [14] A. Beuter, L. Glass, M. Mackey, and M. Titcombe, *Nonlinear Dynamics in Physiology and Medicine* (Springer-Verlag, New York, 2003).
- [15] B. Stone, *Chatter and Machine Tools* (Springer, Berlin, 2014).
- [16] D. M. Kane and K. A. Shore, *Unlocking Dynamical Diversity: Optical Feedback Effects on Semiconductor Lasers* (John Wiley & Sons, New York, 2005).
- [17] M. C. Soriano, J. García-Ojalvo, C. R. Mirasso, and I. Fischer, *Rev. Mod. Phys.* **85**, 421 (2013).
- [18] K. Ikeda, *Opt. Commun.* **30**, 257 (1979).
- [19] K. Ikeda, H. Daido, and O. Akimoto, *Phys. Rev. Lett.* **45**, 709 (1980).
- [20] H. M. Gibbs, F. A. Hopf, D. L. Kaplan, and R. L. Shoemaker, *Phys. Rev. Lett.* **46**, 474 (1981).
- [21] H. Nakatsuka, S. Asaka, H. Itoh, K. Ikeda, and M. Matsuoka, *Phys. Rev. Lett.* **50**, 109 (1983).
- [22] S.-N. Chow and J. Mallet-Paret, *North-Holland Math. Stud.* **80**, 7 (1983).
- [23] J. Mallet-Paret and R. D. Nussbaum, *Ann. Mat. Pura Appl.* **145**, 33 (1986).
- [24] S.-N. Chow, J. K. Hale, and W. Huang, *Proc. Roy. Soc. Edinb. A* **120**, 223 (1992).
- [25] J. Hale and W. Huang, *J. Diff. Equ.* **114**, 1 (1994).
- [26] J. K. Hale and W. Huang, *Z. Angew. Math. Phys.* **47**, 57 (1996).
- [27] M. Nizette, *Physica D* **183**, 220 (2003).
- [28] L. Weicker, T. Erneux, O. D’Huys, J. Danckaert, M. Jacquot, Y. Chembo, and L. Larger, *Philos. Trans. R. Soc. Lond. A* **371** (2013).
- [29] L. Weicker, T. Erneux, O. D’Huys, J. Danckaert, M. Jacquot, Y. Chembo, and L. Larger, *Phys. Rev. E* **86**, 055201(R) (2012).
- [30] G. Friart, L. Weicker, J. Danckaert, and T. Erneux, *Opt. Express* **22**, 6905 (2014).
- [31] L. Weicker, T. Erneux, D. P. Rosin, and D. J. Gauthier, *Phys. Rev. E* **91**, 012910 (2015).
- [32] G. Friart, G. Verschaffelt, J. Danckaert, and T. Erneux, *Opt. Lett.* **39**, 6098 (2014).
- [33] Y. C. Kouomou, P. Colet, L. Larger, and N. Gastaud, *Phys. Rev. Lett.* **95**, 203903 (2005).
- [34] A. B. Cohen, B. Ravoori, T. E. Murphy, and R. Roy, *Phys. Rev. Lett.* **101**, 154102 (2008).
- [35] X. S. Yao and L. Maleki, *Opt. Lett.* **21**, 483 (1996).
- [36] L. Larger, *Philos. Trans. R. Soc. Lond. A* **371** (2013).
- [37] A. Argyris, D. Syvridis, L. Larger, V. Annovazzi-Lodi, P. Colet, I. Fischer, J. Garcia-Ojalvo, C. R. Mirasso, L. Pesquera, and K. A. Shore, *Nature* **438**, 343 (2005).
- [38] J. Lasri, P. Devgan, R. Tang, and P. Kumar, *Opt. Express* **11**, 1430 (2003).
- [39] J. Lasri, P. Devgan, R. Tang, and P. Kumar, *IEEE Photon. Technol. Lett.* **16**, 263 (2004).
- [40] Y. K. Chembo, A. Hmima, P.-A. Lacourt, L. Larger, and J. M. Dudley, *J. Lightwave Technol.* **27**, 5160 (2009).
- [41] R. Martinenghi, S. Rybalko, M. Jacquot, Y. K. Chembo, and L. Larger, *Phys. Rev. Lett.* **108**, 244101 (2012).
- [42] L. Larger, M. C. Soriano, D. Brunner, L. Appeltant, J. M. Gutiérrez, L. Pesquera, C. R. Mirasso, and I. Fischer, *Opt. Express* **20**, 3241 (2012).
- [43] M. Peil, M. Jacquot, Y. K. Chembo, L. Larger, and T. Erneux, *Phys. Rev. E* **79**, 026208 (2009).
- [44] C. M. Bender and S. A. Orszag, in *Advanced Mathematical Methods for Scientists and Engineers* (McGraw Hill, New York, 1978), pp. 544–568.
- [45] J. Kevorkian and J. D. Cole, in *Multiple Scale and Singular Perturbation Methods* (Springer, Berlin, 1996), pp. 267–407.